Compartmental Model of Vertebrate Motoneurons for Ca^{2+}-Dependent Spiking and Plateau Potentials Under Pharmacological Treatment

VICTORIA BOOTH,[1] JOHN RINZEL,[1] AND OLE KIEHN[2]
[1]*Mathematical Research Branch, National Institute of Diabetes and Digestive and Kidney Diseases, National Institutes of Health 9190, Bethesda, Maryland 20814; and* [2]*Section of Neurophysiology, Department of Physiology, The Panum Institute, DK-2200 Copenhagen, Denmark*

Booth, Victoria, John Rinzel, and Ole Kiehn. Compartmental model of vertebrate motoneurons for Ca^{2+}-dependent spiking and plateau potentials under pharmacological treatment. *J. Neurophysiol.* 78: 3371–3385, 1997. In contrast to the limited response properties observed under normal experimental conditions, spinal motoneurons generate complex firing patterns, such as Ca^{2+}-dependent regenerative spiking and plateaus, in the presence of certain neurotransmitters and ion-channel blockers. We have developed a quantitative motoneuron model, based on turtle motoneuron data, to investigate the roles of specific ionic currents and the effects of their soma and dendritic distribution in generating these complex firing patterns. In addition, the model is used to explore the effects of multiple ion channel blockers and neurotransmitters that are known to modulate motoneuron firing patterns. To represent the distribution of ionic currents across the soma and dendrites, the model contains two compartments. The soma compartment, representing the soma and proximal dendrites, contains Hodgkin-Huxley-like sodium (I_{Na}) and delayed rectifier K^+ (I_{K-dr}) currents, an N-like Ca^{2+} current (I_{Ca-N}), and a calcium-dependent K^+ current [$I_{K(Ca)}$]. The dendritic compartment, representing the lumped distal dendrites, contains, in addition to I_{Ca-N} and $I_{K(Ca)}$ as in the soma, a persistent L-like calcium current (I_{Ca-L}). We determined kinetic parameters for I_{Na}, I_{K-dr}, I_{Ca-N}, and $I_{K(Ca)}$ in order to reproduce normal action-potential firing observed in turtle spinal motoneurons, including fast and slow afterhyperpolarizations (AHPs) and a linear steady-state frequency-current relation. With this parameter set as default, a sequence of pharmacological manipulations were systematically simulated. A small reduction of I_{K-dr} [mimicking the experimental effect of tetraethylammonium (TEA) in low concentration] enhanced the slow AHP and caused calcium spiking (mediated by I_{Ca-N}) when I_{Na} was blocked. Firing patterns observed experimentally in high TEA [and tetrodotoxin (TTX)], namely calcium spikes riding on a calcium plateau, were reproduced only when both I_{K-dr} and $I_{K(Ca)}$ were reduced. Dendritic plateau potentials, mediated by I_{Ca-L}, were reliably unmasked when $I_{K(Ca)}$ was reduced, mimicking the experimental effect of the bee venom apamin. The effect of 5-HT, which experimentally induces the ability to generate calcium-dependent plateau potentials but not calcium spiking, was reproduced in the model by reducing $I_{K(Ca)}$ alone. The plateau threshold current level, however, was reduced substantially if a simultaneous increase in I_{Ca-L} was simulated, suggesting that serotonin (5-HT) induces plateau potentials by regulating more than one conductance. The onset of the plateau potential showed significant delays in response to near-threshold, depolarizing current steps. In addition, the delay times were sensitive to the current step amplitude. The delay and its sensitivity were explained by examining the model's behavior near the threshold for plateau onset. This modeling study thus accurately accounts for the basic firing behavior of vertebrate motoneurons as well as a range of complex firing patterns invoked by ion-channel blockers and 5-HT. In addition, our computational results support the hypothesis that the electroresponsiveness of motoneurons depends on a nonuniform distribution of ionic conductances, and they predict modulatory effects of 5-HT and properties of plateau activation that have yet to be tested experimentally.

INTRODUCTION

Vertebrate motoneurons possess a variety of ionic conductances that under normal conditions give rise to a relatively limited firing repertoire characterized by fast action potentials (APs) and smooth rate regulation in response to intracellular current injection or synaptic activation (Binder et al. 1996; Schwindt and Crill 1984). In the presence of certain ion channel blockers or neurotransmitters, more complex firing patterns can be evoked. For example, in serotonin (5-HT) and norepinephrine, cat (Conway et al. 1988; Hounsgaard et al. 1988a; Lee and Heckman 1996b) and turtle motoneurons (Hounsgaard and Kiehn 1989) can be shifted between two stable modes of firing, differing in frequency by up to 10 Hz, by short-lasting excitatory and inhibitory inputs. This bistable firing, which is also found in single-unit recordings in intact animals (Eken and Kiehn 1989), endows motoneurons with a mechanism for translating short-lasting synaptic inputs into long-lasting motor output (see Kiehn 1991b for a review). The recent demonstration that selective depletion of descending monoaminergic fibers from the brain stem to the spinal cord results in a substantial reduction in tonic motoneuron activity in antigravity muscle suggests that monoamine-induced bistable firing is active in the up-right position (Kiehn et al. 1996). When the sodium spike generating mechanism is blocked with tetrodotoxin (TTX), an underlying plateau potential responsible for the bistable firing is revealed. The plateau-generating current has been identified as a persistent, inward, calcium-dependent (Hounsgaard and Kiehn 1985; Schwindt and Crill 1984), and nifedipine-sensitive current (Hounsgaard and Kiehn 1989; Hounsgaard and Mintz 1988), making it likely to be mediated by an L-like calcium conductance. Plateau potentials, similar to those induced by 5-HT and norepinephrine, are also seen after blocking outward potassium currents (Hounsgaard and Mintz 1988; Schwindt and Crill 1980a–c). In particular, the bee venom apamin, which blocks the calcium-dependent K^+ current underlying the slow afterhyperpolarization (AHP) (Hounsgaard et al. 1988b; Zhang and Krnjevic 1987), elicits plateau potentials in turtle motoneurons with an appearance similar to those induced by 5-HT (Hounsgaard and Kiehn 1989; Hounsgaard and Mintz 1988). In contrast, high concentrations of tetraethylammo-

nium (TEA) induce the ability to generate both plateau potentials and Ca^{2+}-based spiking (Hounsgaard and Mintz 1988). The Ca^{2+}-based spiking is most likely mediated by an N-like Ca^{2+} conductance.

The biophysical mechanisms for the induction of these Ca^{2+}-dependent regenerative responses by ion channel blockers and monoamines have not, however, been adequately identified. We have therefore developed a compartmental motoneuron model, based on turtle motoneuron data, to investigate the roles of the ionic currents responsible for these Ca^{2+}-dependent responses and the effect of their soma and dendritic distribution. Some previous models were developed to explore bistable firing in vertebrate motoneurons, including an idealized, equivalent cylinder, cable model (Gutman 1991), an isopotential (or single compartment), threshold-crossing model (Powers 1993), and simple and more detailed two-compartment models (Booth and Rinzel 1995; Lee and Heckman 1996a). The present modeling study, in contrast, is the first to investigate the effects exerted by multiple ion channel blockers and neurotransmitters that account for a variety of complex firing behaviors experimentally observed in turtle motoneurons during a sequence of pharmacological experiments.

The precise effects of 5-HT on the ionic conductances of turtle motoneurons are not known (Hounsgaard and Kiehn 1989, 1993). Its primary effect has been suggested to be a reduction of the Ca^{2+}-dependent K^+ current [$I_{K(Ca)}$] that mediates the slow AHP of APs since there is a visible decrease in the slow AHP in the presence of 5-HT (Hounsgaard and Kiehn 1989). It is known, however, that 5-HT can affect multiple conductances in other vertebrate motoneurons (Kiehn 1991a; McLarnon 1995). We therefore used the model to explore possible effects of 5-HT on conductances other than $I_{K(Ca)}$, such as the L-like Ca^{2+} conductance, which is a logical target for 5-HT given its role in plateau generation. In particular, we investigated and compared changes in plateau properties obtained in the model in response to variation of the Ca^{2+}-dependent K^+ and the L-like Ca^{2+} conductance levels. Varying the maximum conductances for these currents simulated not only different actions of 5-HT on the conductances but also different concentrations of 5-HT, thus predicting experiments that may help distinguish effects of 5-HT on turtle motoneuron conductances.

Finally, the model is used to analyze some key features of the plateau activation, including delays in plateau onset, in some cases lasting over a second, observed in response to near-threshold current steps, and the slow rise of the voltage to the plateau state once plateau activation has been initiated. These voltage and time dependencies of the plateau activation have led to suggestions that the activation time constant of the L-like Ca^{2+} conductance underlying the plateau may be slow in motoneurons, perhaps on the order of 100 ms (Powers 1993; Schwindt and Crill 1984). Our model analysis indicated that these features may be obtained with a relatively fast activation time constant of the plateau-generating current.

Some of these results have been presented in short form (Booth and Rinzel 1996; Booth et al. 1996).

METHODS

General description of the model

The model includes most of the ionic conductances that have been experimentally identified in turtle spinal motoneurons (Hounsgaard et al. 1988b; Hounsgaard and Kiehn 1989; Hounsgaard and Mintz 1988). Sodium (I_{Na}) and potassium delayed rectifier (I_{K-dr}) conductances contribute to AP generation in the standard Hodgkin-Huxley manner. An inactivating, high threshold, N-like calcium conductance (I_{Ca-N}), which is similar to high-voltage–activated Ca^{2+} currents found in cat spinal (Powers 1993; Schwindt and Crill 1984) and in rat hypoglossal motoneurons (Umemiya and Berger 1994; Viana et al. 1993a), allows calcium influx during APs. Also included in the model is a calcium-dependent potassium conductance [$I_{K(Ca)}$] that contributes to the slow AHP following a spike. These four conductances are responsible for AP generation. The final conductance included in the model is a persistent, low-threshold, L-like calcium conductance (I_{Ca-L}), which, in turtle motoneurons, generates plateau potentials observed in the presence of 5-HT and potassium channel blockers. This conductance corresponds to the low-threshold, persistent calcium conductance previously described in cat spinal motoneurons (Schwindt and Crill 1984).

Experimental results in both turtle and cat motoneurons have indicated that active conductances in the dendrites participate in the generation of bistable firing patterns observed in 5-HT and norepinephrine (Hounsgaard and Kiehn 1993; Lee and Heckman 1996b). The turtle motoneuron experiments have further identified both N-like and L-like calcium conductances (Hounsgaard and Mintz 1988) at dendritic locations (Hounsgaard and Kiehn 1993). In our previous, minimal model, we investigated whether the segregation of plateau-generating conductances to a dendritelike compartment that was electrically distal from a sodium spike-generating compartment could account for the bistable firing behavior observed under 5-HT (Booth and Rinzel 1995). The results from the minimal model supported a dendritic origin for the plateau conductance. In the present enhanced model, we retain the two compartment structure of our previous model and the general notion of segregating the sodium-spiking mechanisms from the plateau-generating mechanisms. Figure 1 shows a schematic diagram of the enhanced model. The soma compartment contains the four conductances responsible for the generation of sodium APs, whereas the dendrite compartment holds the two calcium conductances and the calcium-dependent potassium conductance.

For each active conductance in the model, differential equations generate the time and voltage dependencies of the activation and inactivation gates, with Boltzman equations describing their steady-state voltage dependencies. The parameters for the gating kinetics have been qualitatively determined, because precise, quantitative measurements for most parameters are not available for turtle motoneurons (Hounsgaard et al. 1988b; Hounsgaard and Kiehn 1989; Hounsgaard and Mintz 1988). For this study, we assigned parameters based on the qualitative and quantitative measurements available (see following paragraphs) and then tuned these values to obtain good fits with the normal firing behavior and pharmacologically altered behaviors observed experimentally. A listing of the model equations and parameter values is given in the APPENDIX. The results shown in Figs. 2–6 were obtained by numerically integrating the model equations with a variable time-step Gear method (see APPENDIX). In the following paragraphs, we discuss in more detail the kinetics of our model conductances and the electronic-like properties of the model. The sensitivities of our results on parameter values is discussed throughout RESULTS.

Sodium and potassium delayed rectifier conductances

The sodium and potassium delayed rectifier conductances have standard Hodgkin-Huxley-like activation and inactivation kinetics. The sodium conductance is governed by the usual m^3h gating variables with instantaneous activation and time-dependent inactivation. The potassium delayed rectifier conductance activates as n^4, where the gating variable n is both time and voltage dependent. Parameters for the kinetics of these conductances are based on

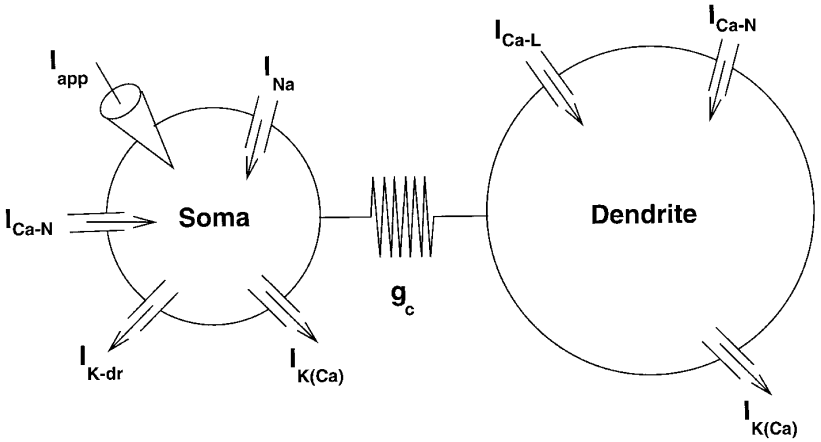

FIG. 1. Schematic diagram of 2-compartment vertebrate motoneuron model. The soma compartment contains ionic conductances that generate action potentials. The dendrite compartment contains conductances responsible for plateau generation. Current spread between the compartments is through the coupling conductance g_c. Model equations and parameter values are given in the APPENDIX.

those from an early, multicompartmental motoneuron model developed by Traub (Traub 1977; Traub and Llinas 1977) but were modified to incorporate more recent data obtained in cat spinal motoneurons (Schwindt and Crill 1984) and rat motoneurons (Takahashi 1990b; Viana et al. 1993b). Some differences in our parameter values from those in Traub's (1977) model include a depolarizing shift in half-activation of the delayed rectifier conductance, hyperpolarizing shifts in the reversal potential for potassium and in sodium half-inactivation, and a slower maximum time constant for sodium inactivation resulting in slower deinactivation of the Na^+ conductance.

N-like calcium conductance

The N-like calcium conductance gating is given by $m_N^2 h_N$ with both activation m_N and inactivation h_N having voltage and time dependencies. Only qualitative data are available for the kinetic parameters of this conductance in turtle motoneurons (Hounsgaard and Mintz 1988), but the parameters describing activation correspond well to those used in a recent model by Powers (1993) to characterize the high-threshold calcium conductance found in cat motoneurons. Our choice for parameter values was influenced by achieving appropriate behaviors in AP and calcium-based spiking.

Calcium-dependent potassium conductance

The calcium-dependent potassium [K(Ca)] conductance activates instantaneously according to the Hill expression with exponent 1

$$\frac{Ca_x}{Ca_x + K_d}$$

where Ca_x ($x = S$ or D) defines the intracellular calcium concentration (in μM) in the soma and dendrite compartments, respectively, and the half-saturation level is given by the constant K_d. The exponent 1 in this expression was fundamental in obtaining a linear frequency-current relation for AP firing. Note that this conductance does not depend on voltage directly, but only indirectly through the calcium conductances mediating Ca^{2+} influx to the compartment.

L-like calcium conductance

The L-like calcium current is persistent with activation determined by the time- and voltage-dependent gating variable m_L. It has a low threshold for activation, below that of our N-like Ca^{2+} conductance, similar to the persistent, low-threshold Ca^{2+} conductance in cat motoneurons and as suggested by plateau behavior in turtle motoneurons (Hounsgaard and Mintz 1988). The time course of activation of the persistent Ca^{2+} conductance in cat motoneurons is slow (Powers 1993; Schwindt and Crill 1984); depending on the strength of activation, it can vary from 30 ms to several 100 ms. Our model simulations, however, do not produce accurate plateau potential profiles with a very slow activation time constant. In particular, with a very large time constant, we obtain plateau activation slopes that are much shallower than experimentally observed. We further discuss the effects of this time constant on the behavior of plateau potentials in RESULTS. For this study, a relatively fast time constant of 40 ms is used.

Intracellular calcium concentration

The intracellular Ca^{2+} concentration (measured in μM) is modeled separately in each compartment according to the following balance equation

$$\frac{dCa_x}{dt} = f[-\alpha I_{Ca} - k_{Ca}Ca_x] \quad (1)$$

where $x = S$ or D for the soma or dendrite compartment, respectively. The constant f is the percent of free to bound Ca^{2+}. The parameter α converts the total Ca^{2+} current in the compartment, I_{Ca}, to Ca^{2+} concentration. (This parameter implicitly contains the ratio of surface area to volume for each compartment, but, because our model crudely reduces neuronal structure to only 2 compartments, a strict geometric interpretation of this parameter is inappropriate.) The constant k_{Ca} represents the Ca^{2+} removal rate, where Ca^{2+} is removed by uptake into internal stores or pump extrusion.

Electrotonic-like properties of the two-compartment model

The electrotonic-like properties of the two-compartment model are determined by two parameters: the coupling conductance g_c, which regulates current flow between the compartments, and the parameter p, which is the ratio of somatic surface area to total surface area. Appropriate values for these parameters cannot be directly derived from geometric and passive electrical properties of motoneurons. To determine these parameters, the nonlinear interactions of the ionic conductances in both compartments must also be considered (see Pinsky and Rinzel 1994 for a discussion). The default value of the parameter p is set to 0.1, estimating that the soma has $^1/_{10}$ the surface area of the entire motoneuron. Although there are no data on the soma/dendrite area ratio for turtle motoneurons, surface area measurements of cat motoneurons range from 250,000 to 750,000 μm^2 with the soma accounting for between 6,000 and 15,000 μm^2 (Lüscher and Clamann 1992). Thus the value of p might be too high, but qualitatively similar results to those described in this study can be obtained with smaller values of p.

The default value of the coupling conductance, $g_c = 0.1$ mS/cm^2, was chosen to provide a fairly weak coupling current between

compartments, which was determined necessary to generate a bistable firing behavior in previous two-compartment models (Booth and Rinzel 1995; Lee and Heckman 1996a). This value of g_c yields much greater voltage attenuation in the dendrite compartment in response to steady somatic depolarization than has been experimentally estimated in vertebrate motoneurons. For example, dendritic voltage in our model under control conditions displays ~70% decay compared with estimates of 15–40% decay in distal, passive dendrites of cat gamma motoneurons (Burke et al. 1994) and estimates of 20% decay in distal, passive dendrites of guinea pig vagal motoneurons (Nitzan et al. 1990) in response to steady somatic depolarization. However, larger values of g_c, which reduce the steady voltage attenuation observed in the dendrite compartment under control conditions, destroy plateau potential generation when 5-HT is simulated. For example, when g_c was doubled (g_c = 0.2 mS/cm^2), which yielded a voltage attenuation in the dendrite compartment of 51%, the model displayed plateau potentials only in a very narrow range of applied current values that did not correspond to experimental observations. Furthermore, when g_c was tripled (g_c = 0.3 mS/cm^2), steady voltage attenuation in the dendrite compartment showed a 42% decay, but the model did not display bistable firing behavior for any applied current values.

RESULTS

As a first test of the robustness of our model, we searched for a set of maximum conductance density values that reproduce normal spiking behavior in response to long-lasting current steps. This set of control conductance densities is given in Table 1. The effect of ion channel blockers and neurotransmitters was then simulated by varying these control conductance values in a systematic manner to account for a sequence of pharmacological experiments.

Normal spiking behavior

With the control conductance values, the model displays spiking behavior that resembles normal experimental AP firing. Figure 2*A* shows low-frequency firing obtained with the model in response to an injected current pulse near the firing threshold. Note that the full-sized AP generated in the soma compartment (*top trace*) invokes a small excursion in dendritic voltage (*middle trace*). The model APs possess the distinctive features observed in turtle motoneuron APs, namely a fast AHP associated with spike repolarization and a delayed, slow AHP governing the return to spike threshold. These two AHPs reflect the action of the two potassium currents in the soma compartment. The delayed rectifier current, which contributes to AP repolarization, is responsible for the fast AHP, whereas the slow AHP is mediated by $I_{K(Ca)}$. (To better understand the contributions of the individual ionic currents to AP generation, a dissection of an AP is shown in Fig. A1 in the APPENDIX.) The contribution of the two potassium conductances to spike profile is illustrated by a comparison of the higher frequency control APs in Fig. 2*B* with those in Fig. 2*D*, where a low concentration of TEA is simulated by reducing I_{K-dr} by 66%. As observed experimentally in turtle motoneurons, a low concentration of TEA eliminates the fast AHP (compare Fig. 2*D* with Fig. 1*B* in Hounsgaard and Mintz 1988). The elimination of the fast AHP has a series of consequences that results in the lower frequency firing observed in simulated TEA. Specifically, each spike is wider with an increased Ca^{2+} component, mediated by I_{Ca-N}, that allows more calcium to enter the compartment. The elevated concentration of intracellular Ca^{2+} causes increased activation of $I_{K(Ca)}$ and thus a more substantial slow AHP, leading to decreased frequency in response to the same amplitude current step. These model results are also similar to changes in AP profile observed in response to TEA in rat hypoglossal motoneurons (Viana et al. 1993b).

TABLE 1. *Control values of maximum conductance densities*

Maximum Conductance	Soma Compartment	Dendrite Compartment
g_{Na}	120	
g_{K-dr}	100	
g_{Ca-N}	14	0.3
$g_{K(Ca)}$	5	1.1
g_{Ca-L}		0.33

Values are in mS/cm^2. The effect of pharmacological agents is simulated by changing these control conductances in an appropriate manner. The specific parameter variations are given in the legends of Figs. 2–9.

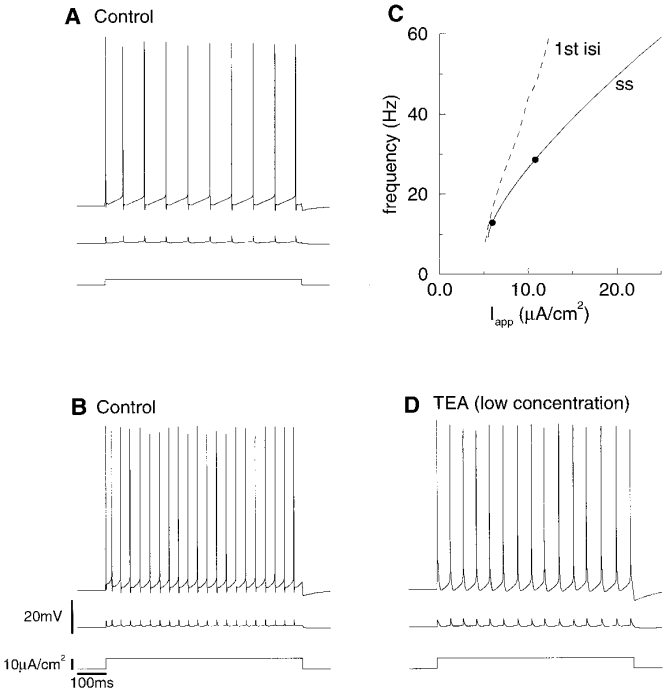

FIG. 2. Sodium spike behavior obtained in model under control conditions and in simulated tetraethylammonium (TEA). *A, B,* and *D*: voltage responses measured in soma (*top trace*) and dendrite (*middle trace*) compartments shown in response to injected current pulse (*bottom trace*). *A* and *B*: normal sodium action-potential firing in control conditions in response to near-threshold (*A*, I_{app} = 6 μA/cm^2) and larger current steps (*B*, I_{app} = 11 μA/cm^2). *C*: steady-state (solid) and 1st interspike interval (dotted) frequency-current relations for action-potential firing. Filled circles indicate steady-state frequencies in *A* and *B.* Figures 2–9 and A1: control conductance density values (Table 1) used except where noted. *D*: sodium-based spikes obtained in simulated low-concentration TEA (g_{K-dr} = 34 mS/cm^2, I_{app} = 11 μA/cm^2).

In vertebrate motoneurons, the steady-state frequency of AP firing increases in a piecewise linear fashion in response to increasing applied current (Baldissera and Gustafsson 1974; Binder et al. 1996; Kernell 1965; Schwindt and Crill 1984). For example, as current levels are increased from firing threshold, the steady-state frequency increases linearly with a shallow slope through a primary range until the slope

abruptly increases to define a secondary range. Our model operates only in the primary range of AP frequencies. As shown in the frequency-current (*f-I*) plot in Fig. 2*C*, except for a steep initial gradient, the steady-state frequency (solid) increases essentially linearly from firing threshold. (The steady-state frequencies attained in the simulations shown in Fig. 2, *A* and *B*, are indicated by the filled circles). The voltage trajectories between spikes obtained with the model display similar behavior as has been noted experimentally as frequency increases in the primary range (Schwindt and Calvin 1972). The slope of the voltage rise to spike threshold remains constant as frequency increases, but the slow AHP begins at progressively more depolarized levels, leading to a progressively shorter rise to threshold (compare Fig. 2, *A* and *B*).

Another characteristic of motoneuron AP firing is the adaptation in firing frequency that takes place after an injected current step. Under normal conditions, the frequency is observed to decrease steadily throughout a current step, with a fast initial adaptation followed by a slower adaptation that may continue for several seconds (Kernell and Monster 1982). Our model displays a frequency adaptation over the first few spike intervals after a current step, evidenced by the steeper slope of the first interspike interval *f-I* curve shown dashed in Fig. 2*C*. The exact mechanism for the slow adaptation observed in motoneurons is not known (Binder et al. 1996), and in this model we were only able to obtain a fast, initial adaptation caused by a slow build-up of intracellular calcium during the first few spikes following a current step that leads to a progressive increase in the slow AHPs.

Ca^{2+}-based regenerative responses

The two distinct Ca^{2+} conductances identified in turtle motoneurons, an N-like and an L-like conductance (Hounsgaard and Mintz 1988), are balanced by outward K^+ currents under normal conditions, but in the presence of K^+ channel blockers, they induce changes in AP profile and can generate new firing behaviors.

In turtle motoneurons, the N-like Ca^{2+} current is evident under normal conditions only by the transient influx of Ca^{2+} during an AP (Hounsgaard and Mintz 1988). Its contribution to more complex firing patterns has been determined experimentally in the presence of a low concentration of TEA. When the Na^+ current was blocked by the addition of TTX in the experimental preparation, the N-like conductance generated Ca^{2+}-based spikes in response to a depolarizing current step (Hounsgaard and Mintz 1988). In the model, similar Ca^{2+}-based spikes are obtained under simulation of both TTX (I_{Na} reduced by ~90%) and low concentration TEA (I_{K-dr} reduced by 66%), as shown in Fig. 3*A*. In the figure, a large current step induces Ca^{2+}-based spikes that are smaller in amplitude and much wider than normal Na^+ spikes. These Ca^{2+}-based spikes show a slow, smooth increase to firing threshold governed by $I_{K(Ca)}$ and reflecting the removal of intracellular Ca^{2+}. In the turtle experiments, a much larger current step was necessary to invoke Ca^{2+} spikes than was needed to induce Na^+ AP firing. Similarly, the Ca^{2+} spikes obtained in rat hypoglossal motoneurons under treatment by TTX and TEA are also high threshold (Viana et al. 1993a). We have incorporated these experimental results into the kinetic parameters for I_{Ca-N} by making its half-activation more depolarized than the half-activation for I_{Na}.

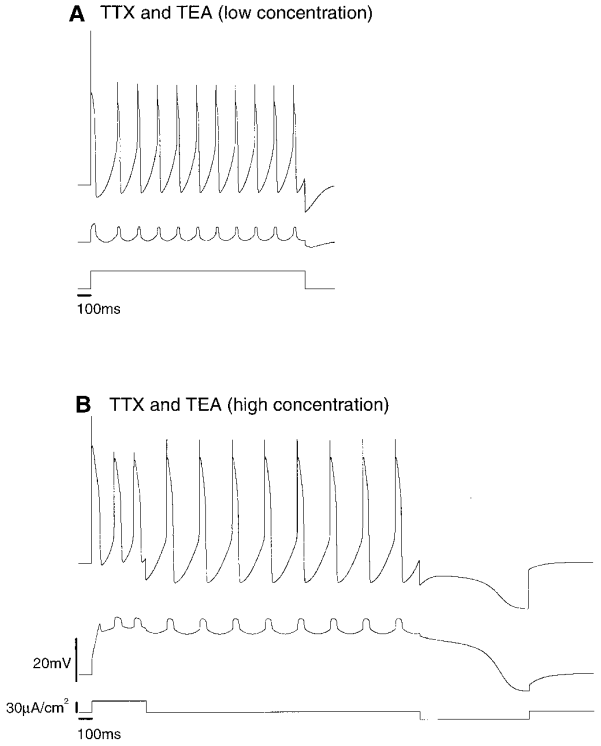

FIG. 3. Calcium-based spikes and plateaus obtained in simulated tetrodotoxin (TTX) and TEA. *A* and *B*: *top* and *middle traces* show voltages measured in soma and dendrite compartments, respectively, in response to applied current pulses (*bottom trace*). *A*: Ca^{2+} spikes invoked by large current step (I_{app} = 55 $\mu A/cm^2$) under simulated TTX and a low concentration of TEA (g_{Na} = 13 and g_{K-dr} = 34 mS/cm^2). *B*: in simulated high-concentration TEA, Ca^{2+}-based plateau leading to bistable Ca^{2+} spikes obtained in response to brief depolarizing (I_{app} = 35 $\mu A/cm^2$) and hyperpolarizing (I_{app} = −25 $\mu A/cm^2$) current pulses (g_{Na} = 13, g_{K-dr} = 10 and $g_{K(Ca)}$ = 0.63 mS/cm^2).

The model behaviors in simulated low concentration TEA, namely wider Na^+ spikes (Fig. 2*D*) and, when I_{Na} is blocked, Ca^{2+}-based spikes (Fig. 3*A*), were sensitive to the manner in which TEA was simulated. For example, if TEA was simulated by blocking less I_{K-dr} than in Figs. 2*D* and 3*A*, then calcium currents could not overcome I_{K-dr} to yield calcium spikes when the Na^+ conductance was reduced. On the other hand, if TEA was simulated by blocking more I_{K-dr}, so that calcium spikes were more easily obtained in the TTX case, the sodium spikes (in low TEA, Fig. 2*D*) displayed a significant Ca^{2+} component, up to tens of milliseconds wide, which was visible as a distinct shoulder on the downstroke of the spike.

In turtle motoneurons, when more K^+ currents are blocked with a much higher concentration of TEA and the sodium current is blocked by TTX, the invoked Ca^{2+} spikes ride on a plateau potential that can be triggered by short-lasting excitation and terminated by short-lasting inhibition (Hounsgaard and Mintz 1988). In the model, similar behavior is obtained when high concentration TEA is simulated by reducing I_{K-dr} by 90% and $I_{K(Ca)}$ by 43% (Fig. 3*B*). The motivation for simulating the effects of high concentration TEA in this manner is addressed in the DISCUSSION in comparison to the unmasking of plateau potentials by the bee

venom apamin. In Fig. 3*B*, a large current pulse invokes a dendritic plateau potential as well as Ca^{2+} spikes. The plateau potential persists after pulse termination leading to prolonged Ca^{2+} spiking (compare with Fig. 2*C* in Hounsgaard and Mintz 1988). A brief, hyperpolarizing current pulse terminates the dendritic plateau potential, and the soma voltage reflects its slow decay.

Bistable firing patterns

In the presence of apamin or 5-HT, motoneurons display a distinctive pattern of AP firing in response to a depolarizing current step. In contrast to the normal frequency adaptation during which the frequency continually decreases over the current step, in the presence of either of these agents, the frequency shows an initial decrease over the first few spikes but then accelerates (Hounsgaard and Kiehn 1989). In addition, an afterdepolarization may maintain AP firing after the stimulus is removed. This firing behavior is explained by activation of a plateau potential mediated by an L-like Ca^{2+} current. Because the precise action of 5-HT on turtle motoneuron ionic conductances is not known, we will first describe the model results under simulated apamin, which is known to be a relatively selective blocker of a Ca^{2+}-dependent K^+ conductance in motoneurons (Hounsgaard et al. 1988b; Viana et al. 1993b; Zhang and Krnjevic 1987). In the model, simulating apamin by reducing $I_{K(Ca)}$ by ~40% (in both the soma and dendrite compartments) unmasks I_{Ca-L} and allows the dendrite to depolarize (Figs. 4 and 5). This is shown in Fig. 4, *A–C*, where a current step invokes repetitive firing that shows a brief frequency adaptation over the first few spikes (*top trace*). Hundreds of milliseconds after this initial adaptation, the frequency accelerates in response to the activation of a plateau potential in the dendrite (*middle trace*) (compare with Fig. 2 in Hounsgaard and Kiehn 1989). When the current pulse is terminated, the dendritic plateau persists, inducing continued steady spiking in the soma. For larger current steps in Fig. 4, *B* and *C*, the onset of the frequency acceleration occurs earlier, reflecting the voltage dependence of plateau activation. Figure 4, *C–F*, displays the voltage dependence of the dendritic plateau termination. In these simulations, the current is stepped to a fixed level from successively more hyperpolarized holding levels. At zero holding current (Fig. 4*C*), the dendritic plateau persists after the current pulse. With a hyperpolarized holding current, the dendritic plateau decays after the pulse causing a decrease in spike frequency and eventual termination of spiking (Fig. 4*D*). With more hyperpolarized holding

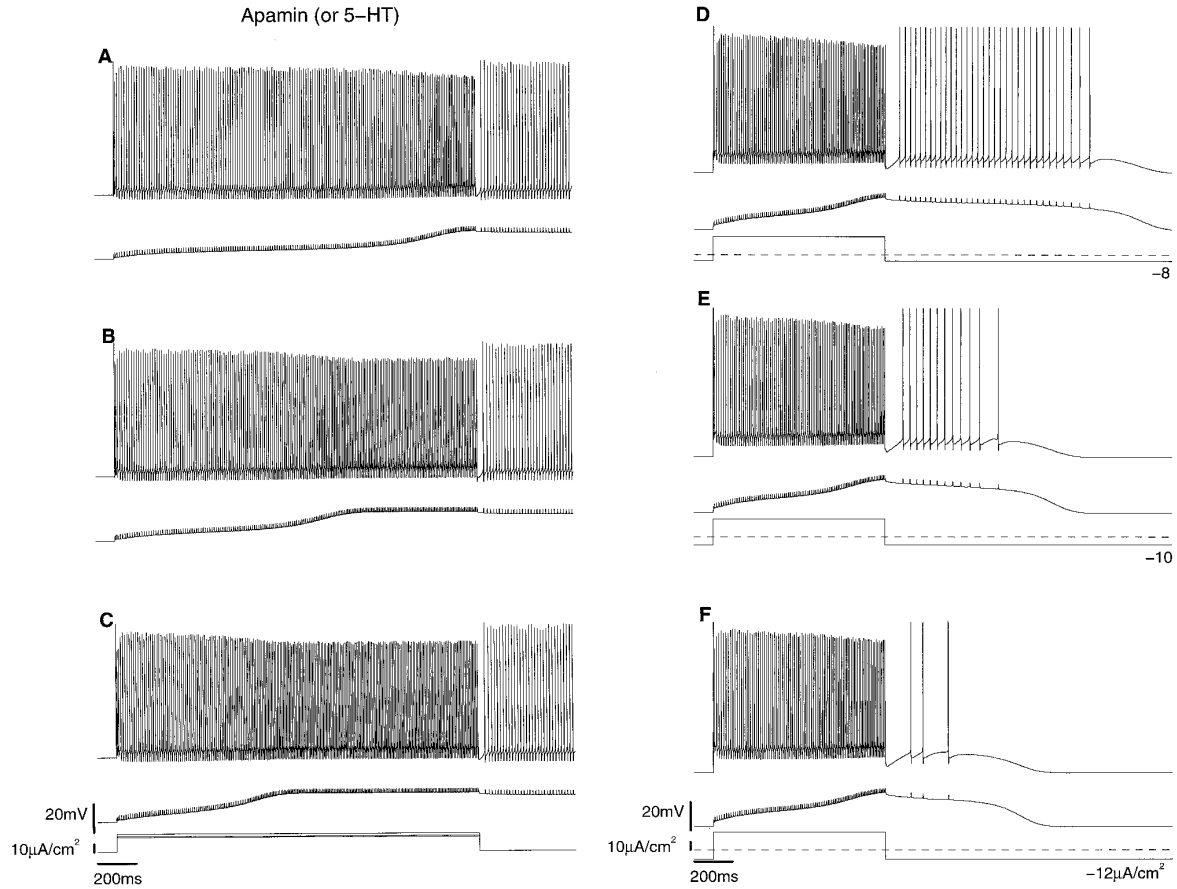

FIG. 4. Bistable firing patterns obtained in simulated apamin [or serotonin (5-HT)]. *A–F*: *top* and *middle traces* show voltages measured in soma and dendrite compartments, respectively, in response to applied current pulses (*bottom trace*). *A–C*: voltage dependence of plateau potential activation displayed by its progressively earlier onset in response to current steps of increasing amplitude (all current traces in *C; A*: I_{app} = 18.5; *B*: I_{app} = 21; *C*: I_{app} = 23 $\mu A/cm^2$ from zero holding current). *D–F*: voltage dependence of plateau termination shown by decay of plateau at hyperpolarized holding currents. Plateau is invoked by current steps to a fixed level (I_{app} = 23 $\mu A/cm_2$) from increasingly hyperpolarized holding currents (*A*: −8; *B*: −10; *C*: −12 $\mu A/cm^2$). *A–F*: soma $g_{K(Ca)}$ = 3.136; dendrite $g_{K(Ca)}$ = 0.69 mS/cm^2.

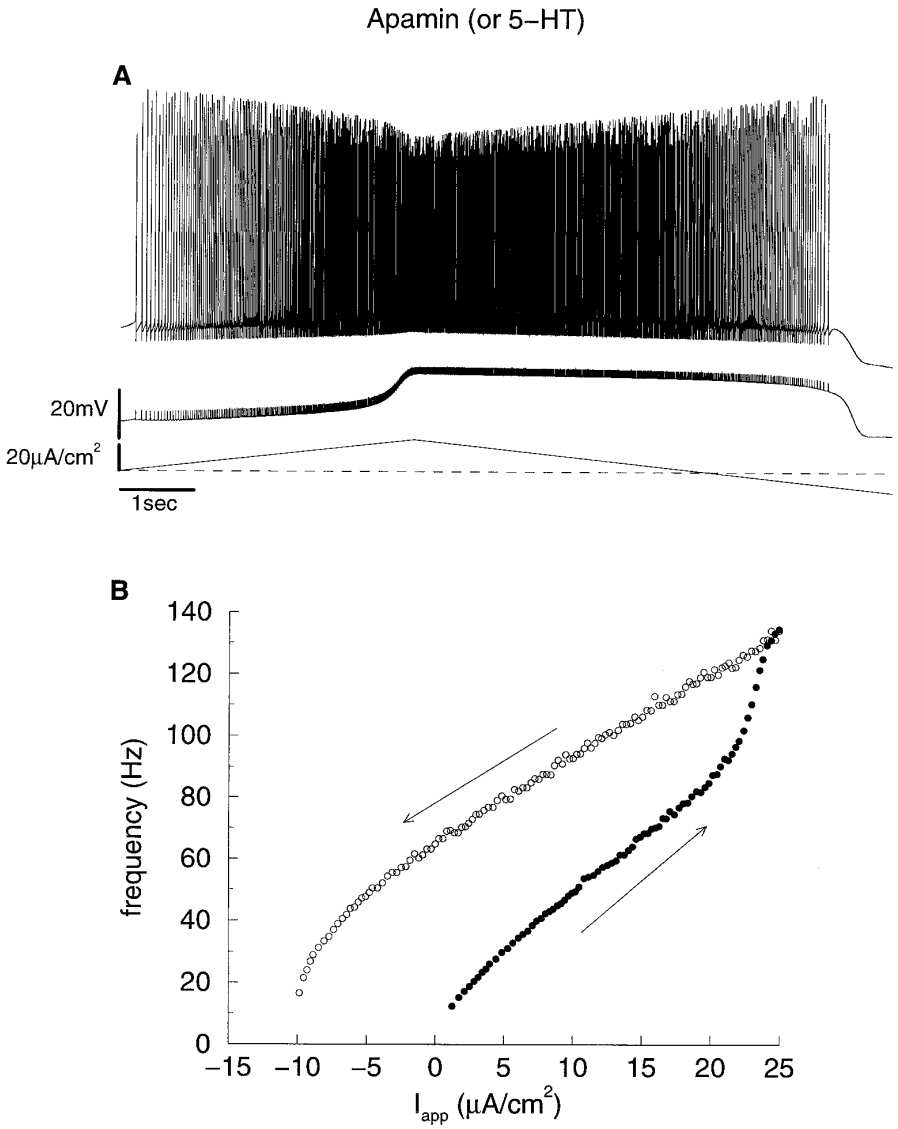

FIG. 5. Bistable firing patterns in response to an injected current ramp obtained in simulated apamin (or 5-HT). *A*: voltage response measured in the soma (*top trace*) and the dendrite (*middle trace*) compartments to injected current that is ramped up and down (*bottom trace*, peak $I_{app} = 25$ $\mu A/cm^2$ reached in 4 s). *B*: instantaneous frequency computed during the ascending (●) and descending (○) phases of the current ramp. Soma $g_{K(Ca)} = 3.136$; dendrite $g_{K(Ca)} = 0.69$ mS/cm^2.

currents, the dendritic plateau and somatic spiking decay more quickly after pulse termination (Fig. 4, *E* and *F*).

With reduced $I_{K(Ca)}$, the model displays the full spectrum of firing behaviors experimentally observed in apamin and 5-HT, including the response to an injected current ramp, which is depicted in Fig. 5 (compare with Fig. 5 in Hounsgaard et al. 1988a). As the current slowly increases in the ascending phase of the current ramp, AP firing in the soma commences, driving small amplitude responses in the dendrite. As the average dendritic voltage level increases, a dendritic plateau potential is activated, causing a jump in spike frequency. This jump is clearly seen in the instantaneous frequency-current plot in Fig. 5*B* during the ascending phase of the ramp (●). Immediately after the jump, the current is ramped back down. The frequency remains at an elevated level during the down ramp (○), and spiking ceases at a level more hyperpolarized than the start of the ascending ramp. In this simulation, the different types of bistable behaviors displayed by the model under simulated apamin or 5-HT can be explored. In a range of currents more negative than zero, where only spiking on the down ramp is observed, the model shows ''bistability'' between a steady voltage state and a steady repetitive firing state. In the range of currents seen on the up ramp between the threshold for firing onset and plateau activation, the model shows another type of bistability: two stable modes of firing. The low-frequency mode corresponds to when the dendrite is near its stable resting state (●), and the high-frequency mode corresponds to when the dendritic plateau is activated (○). If the current is clamped in this range, the bistable firing can be explicitly demonstrated by flipping back and forth between the low- and high-frequency firing modes with brief depolarizing and hyperpolarizing current pulses (simulations not shown).

A feature of 5-HT or apamin modulation of motoneuron firing, in contrast to TEA effects, is that both 5-HT and apamin induce Ca^{2+}-dependent plateau behavior but not calcium spiking under TTX (Hounsgaard and Mintz 1988). This is also the case in the model under simulated apamin, as seen in Fig. 6, where TTX is simulated by completely blocking I_{Na} (compare with Fig. 3 in Hounsgaard and Kiehn 1989). In this case, I_{Ca-N} in the soma cannot overcome the control strength I_{K-dr} to generate Ca^{2+} spiking, and the somatic voltage mimics the plateau responses generated in the dendrite. This is illustrated in Fig. 6*A*, which shows

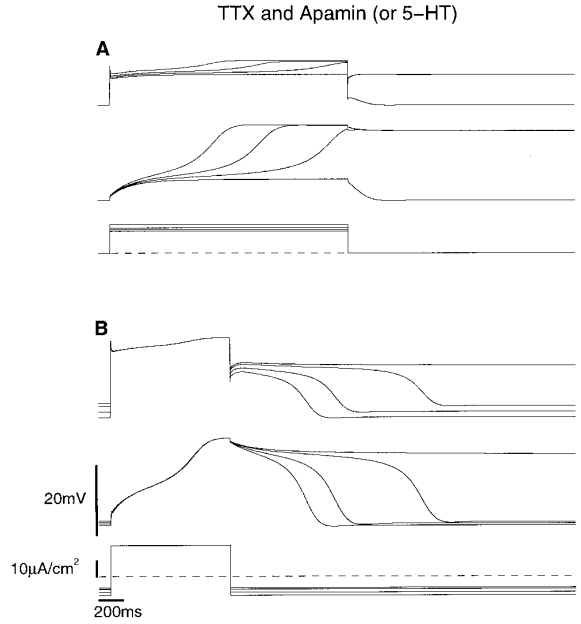

FIG. 6. Plateau potentials obtained in simulated TTX and apamin (or 5-HT). *A* and *B*: *top* and *middle traces* show superimposed voltage trajectories measured in soma and dendrite compartments, respectively, in response to several applied current pulses (*bottom trace*). *A*: onset of plateau potential is increasingly delayed as current step amplitude decreases toward threshold (I_{app} = 18, 16, 15, 14 $\mu A/cm^2$ from zero holding current). *B*: plateau potential, invoked by current steps to a fixed level (I_{app} = 20 $\mu A/cm^2$), decays when current is stepped down to increasingly hyperpolarized holding levels (−7, −8, −10, −12 $\mu A/cm^2$). $g_{Na} = 0$; soma $g_{K(Ca)} = 3.136$; dendrite $g_{K(Ca)} = 0.69$ mS/cm^2.

superimposed voltage responses (soma and dendrite compartments in the *top* and *middle traces*, respectively) to applied current pulses of increasing amplitude (*bottom trace*). For the smallest current pulse, the plateau is not activated; voltage remains steady at a subthreshold level, and at pulse termination, the voltage quickly returns to rest. When the current is stepped just above threshold, plateau activation is significantly delayed, due to the slow increase in voltage from the subthreshold level, and the plateau persists when the stimulus is removed. For larger current steps, plateau onset occurs progressively earlier with the voltage increasing more quickly from the subthreshold level. This delay in plateau onset and its sensitivity to current step amplitude have also been experimentally observed, and a theoretical explanation is presented in a following section. In the simulations shown in Fig. 6*B*, the current is stepped to a fixed level from increasingly more hyperpolarized holding currents, demonstrating that plateau termination occurs earlier when the holding current is more hyperpolarized.

Exploration of 5-HT induction of plateau properties

In this section, we explore possible ways 5-HT may induce plateau properties by modulating multiple conductances. In particular, we investigate changes in plateau properties obtained in the model under simulated TTX in response to variation of $I_{K(Ca)}$ and compare this behavior to plateaus obtained when both $I_{K(Ca)}$ and I_{Ca-L} are varied.

An easily quantifiable property of the plateau response, that can be monitored as parameters are varied, is the plateau onset threshold, that is, the minimum applied current level necessary to invoke the plateau. In this section, we characterize the plateau threshold's dependence on the balances of $I_{K(Ca)}$ and I_{Ca-L} in the model. In both the model and experiment, the onset threshold, I_{onset}, can be estimated by conducting a series of current step simulations, starting with subthreshold step amplitudes and incrementally increasing the amplitude of successive steps until the plateau is fully activated, similar to the simulations shown in Fig. 6*A*. The smallest current step amplitude that invokes the plateau defines I_{onset}. Similarly, the plateau offset threshold, I_{offset}, can be estimated as the least hyperpolarized current level that allows a plateau, as in the simulations in Fig. 6*B*. However, a more precise determination of the plateau thresholds can be obtained by examining the steady-state current-voltage (*I-V*) relation. A cell displaying plateau potentials necessarily possesses an N-shaped steady-state *I-V* relation. The plateau onset threshold corresponds to the knee of the curve that initiates the negative-slope region. The plateau offset threshold, on the other hand, corresponds to the knee that terminates the negatively sloped region. The following section examines in more detail the correspondence between the plateau thresholds and the knees of the steady-state *I-V* curve in terms of the model and, in addition, investigates how the cable properties of the model, as determined by the two compartments, distort the *I-V* curve and the implications for voltage-clamp and current-clamp behaviors.

By tracking the plateau thresholds, I_{onset} and I_{offset}, as $I_{K(Ca)}$ and I_{Ca-L} are varied, we can monitor the emergence of the plateau potential in response to simulated 5-HT. We consider, first, 5-HT only blocking $I_{K(Ca)}$. The curves in Fig. 7*A* show how I_{onset} and I_{offset} change as $I_{K(Ca)}$ is decreased in both the soma and dendrite compartments from 100% (control values) to 50%, simulating an increasing concentration of 5-HT. As $I_{K(Ca)}$ is decreased from its control values (100%), the steady-state *I-V* curve remains monotonic until $I_{K(Ca)}$ is reduced by ~28%. At this point, the curves representing the values of I_{onset} and I_{offset} meet at a cusp, indicating that a very small, N-shaped kink develops in the steady-state *I-V* curve, with a small negative slope region that keeps the knees very close together. As $I_{K(Ca)}$ is further reduced, I_{onset} and I_{offset} move farther apart, depolarizing the plateau state from the subthreshold state and increasing the current range over which a plateau is observed. The emerging plateau becomes discernible under current-clamp conditions when the voltage displacement of the plateau is sufficiently large. The shaded region denotes the levels of $I_{K(Ca)}$ reduction that allow expression of plateaus showing a voltage displacement greater than 2 mV. The filled circles mark I_{onset} and I_{offset} for the TTX and 5-HT simulation in Fig. 6. Note that in this case, I_{offset} is negative so that the plateau persists at zero applied holding current, as in Fig. 6*A*. As $I_{K(Ca)}$ decreases below 60% of its control values, I_{onset} approaches zero current values; when I_{onset} is zero or negative, the plateau spontaneously activates with no stimulation, and near-rest voltage levels can only be obtained with steady hyperpolarizing applied current. From this figure, we can determine that when 5-HT is simulated by decreasing $I_{K(Ca)}$ only, it must reduce this conductance by at least 28% to invoke an N-shaped steady-state relation. It is also clear from this figure that the plateau thresholds, I_{onset} and I_{offset}, are sensitive to the level of K(Ca) conductance and, thereby, the simulated concentration of 5-HT.

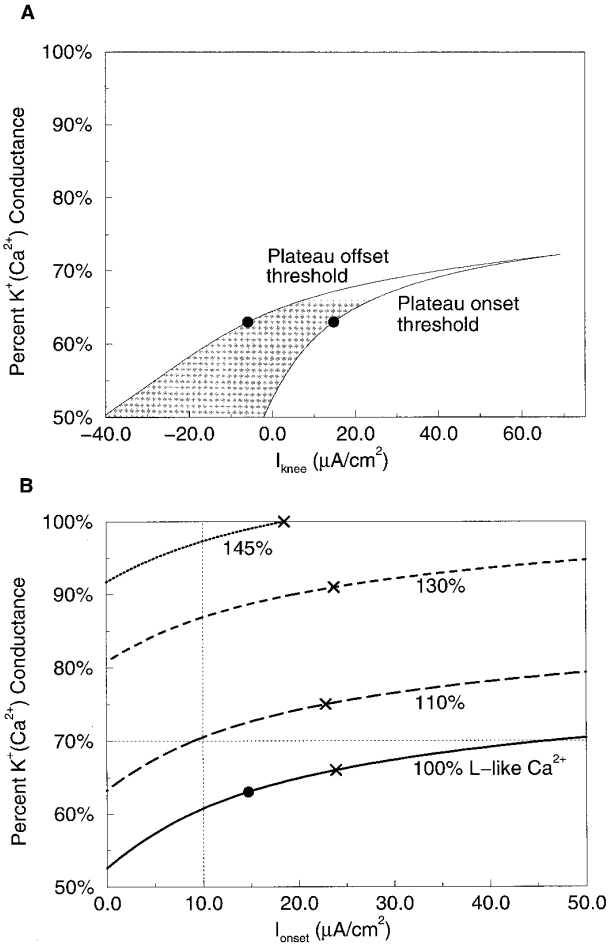

FIG. 7. Plateau properties in response to proposed effects of 5-HT. *A*: curves showing plateau onset thresholds, I_{onset}, and offset thresholds, I_{offset}, defined as the knees of the steady-state current-voltage (*I-V*) curve (see Fig. 8*A*), as increasing concentration of 5-HT is simulated by decreasing the calcium-dependent K^+ conductances in the soma and dendrite compartments (TTX simulated by $g_{Na} = 0$ mS/cm^2). Shaded region indicates conductance values yielding plateaus with at least 2-mV voltage displacement. *B*: curves showing I_{onset} for 5-HT simulated by reduction of $I_{K(Ca)}$ and enhancement of L-like Ca^{2+} conductance (solid, control $g_{Ca-L} = 0.33$; long dashed, $g_{Ca-L} = 0.363$; short dashed, $g_{Ca-L} = 0.429$; dotted, $g_{Ca-L} = 0.4785$ mS/cm^2. TTX simulated by $g_{Na} = 0$ mS/cm^2). Portion of curve below x's corresponds to shaded region in *A*. *A* and *B*: filled circles denote I_{onset} and I_{offset} values for 5-HT simulation in Fig. 6.

To compare plateau properties when 5-HT is simulated as regulating more than one conductance, we track the current value of I_{onset} as the maximum conductance levels of $I_{K(Ca)}$ and I_{Ca-L} are varied. In particular, we consider 5-HT acting to simultaneously block $I_{K(Ca)}$ and enhance I_{Ca-L}, simulating the recruitment of L-like Ca^{2+} channels. The heavy lines in Fig. 7*B* show the change in I_{onset} as $I_{K(Ca)}$ is decreased from 100% (control values) to 50% for increasing levels of I_{Ca-L}. The solid line shows the location of I_{onset} when the L-like calcium conductance is fixed at its control value and only K(Ca) conductance is decreased. This curve is the same as in Fig. 7*A*, but is displayed over a smaller current range. The other curves show the values of I_{onset} when the L-like Ca^{2+} conductance is increased by 10% (long dashed), 30% (short dashed), and 45% (dotted). The ''x'' on each curve denotes the level of $I_{K(Ca)}$ reduction necessary to invoke plateaus with voltage displacement of at least 2 mV (as in the shaded region in Fig. 7*A*), and the filled circle denotes the 5-HT simulation in Fig. 6.

By comparing these curves, we can determine how the plateau onset threshold changes under different combinations of effects of 5-HT. For example, to obtain a plateau threshold at a fixed current level, say 10 μA/cm^2 (thin dotted vertical line), 5-HT has to decrease $I_{K(Ca)}$ ~40% if it affects no other conductance. On the other hand, it reveals plateaus with the same activation threshold by reducing $I_{K(Ca)}$ by only 30% if it also increases I_{Ca-L} by 10%. Similarly, if 5-HT increases I_{Ca-L} by 30 or 45%, a plateau with the same threshold can be unmasked with even smaller reductions in $I_{K(Ca)}$. We can also compare plateau thresholds if 5-HT reduces $I_{K(Ca)}$ by a fixed amount, say 30% (thin dotted horizontal line). In this case, the plateau induced by only $I_{K(Ca)}$ reduction has a much higher threshold than the plateau induced if 5-HT also increases I_{Ca-L} by 10%. Finally, the figure shows that if 5-HT increases I_{Ca-L} by 45%, an observable plateau is induced with no decrease in $I_{K(Ca)}$.

Biophysical determination of plateau thresholds

This section supplements the brief description of the correspondence between the plateau thresholds and the steady-state *I-V* curve given in the beginning of the previous section. In addition, in this section, we investigate how the distortion of the steady-state *I-V* curve due to the cable properties of the model affects behaviors obtained under voltage clamp and current clamp. We illustrate the relation between the steady-state *I-V* curve and the plateau thresholds by considering the model behavior under simulated TTX and 5-HT [modeled by reducing K(Ca) conductances by ~40%, as in Fig. 6]. The theoretical steady-state IV relation for this case (control $g_c = 0.1$ mS/cm^2), is shown by the heavy curve in Fig. 8*A*. The relation is N-shaped with multiple voltage levels for current fixed in a certain range, corresponding to the plateau potential. In addition, the curve also shows multiple current levels for voltage fixed in some range. This latter type of distortion of the curve is due to the cable properties of the model with active currents in the dendrite compartment that are not controlled by a somatic voltage clamp (see p. 401–413 in Jack et al. 1983). The steady-state *I-V* curve was computed in the model as the solutions, including both stable (solid portions of the curve) and unstable (dashed portion) solutions, to the steady-state cable equation for all values of somatic applied current, I_{soma}, using the bifurcation analysis program AUTO (Doedel 1981) (see APPENDIX).

To understand how ''cable effects'' distort the *I-V* relation, Fig. 8*A* also displays the *I-V* curves for the model when the compartments are more tightly coupled (dashed: $g_c = 0.15$, dotted: $g_c = 0.2$ mS/cm^2). These *I-V* curves are N-shaped (that is, showing multiple voltage levels for fixed current), but there is no cable-effect distortion causing multiple current levels for some fixed voltages. The distortion is absent when the compartments are very tightly coupled (dotted curve) because, in this case, the dendrite voltage is essentially equal to the clamped soma voltage and thus active currents in the dendrite compartments are controlled. With the compartments more loosely coupled (dashed curve), the distortion to the negative slope region of the curve begins to appear.

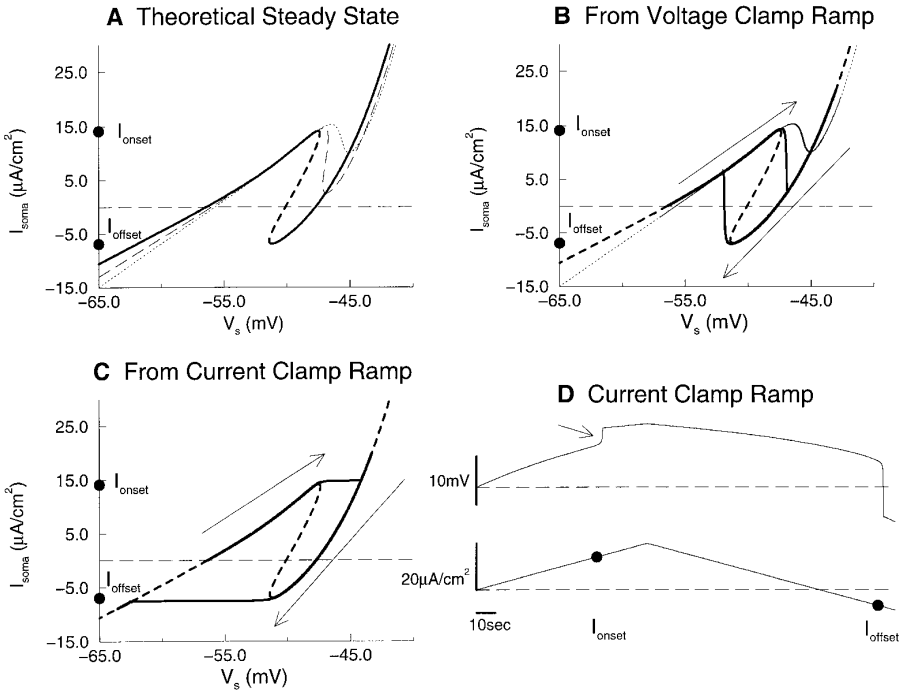

FIG. 8: *I-V* relations obtained in the model under simulated TTX and 5-HT. *A*: theoretical steady-state *I-V* curves computed in the model. Progressive distortion of *I-V* relation caused by cable properties of the model shown by comparing curves for weak control coupling conductance (solid heavy, $g_c = 0.1$) and tighter coupling strengths (dashed, $g_c = 0.15$; dotted, $g_c = 0.2$ mS/cm^2). [*A–D*: TTX and 5-HT simulated by $g_{Na} = 0$, soma $g_{K(Ca)} = 3.136$, and dendrite $g_{K(Ca)} = 0.69$ mS/cm^2.] Plateau potential onset and offset threshold current levels determined by knees of control *I-V* curve and denoted as I_{onset} and I_{offset}, respectively. *B*: *I-V* relations computed by a slow, somatic voltage-clamp ramp for control (heavy, $g_c = 0.1$) and tighter coupling conductances (thin, $g_c = 0.2$ mS/cm^2; arrows denote direction of ramp; V_s ramped from −60 to −40 mV and back in 2 min). Theoretical steady-state *I-V* curves (dashed and dotted) shown for reference. *C* and *D*: somatic current-clamp simulation. *D*: time courses of soma voltage (*top trace*) and applied current (*bottom trace*, peak $I_{app} = 20$ μA/cm^2 reached in 10 s). *C*: same trajectory as in *D* plotted in the somatic *I-V* plane. Voltage jumps corresponding to plateau onset and plateau offset occur as the current is ramped through I_{onset} (arrow in *D*) and I_{offset}, respectively.

The cable-effect distortion seen in the theoretical steady-state *I-V* curve is manifested in a different way when the *I-V* curve is determined by a voltage-clamp ramp (Fig. 8*B*). In the figure, instead of showing the time courses explicitly, we plot the current measured in the soma compartment (solid) against the somatic voltage while it is slowly ramped up and down (arrows indicate direction of the voltage ramp) for the control value of the coupling conductance (heavy curve) and with the compartments more tightly coupled (thin curve, $g_c = 0.2$ mS/cm^2). The dashed and dotted lines are the theoretical steady-state *I-V* curves (from Fig. 8*A*) shown for reference. In both simulations, the voltage is ramped up from near resting potential, and the current increases along the steady-state curve. With the compartments more tightly coupled, the current continues to follow the steady-state curve, sampling the negative-slope region as the voltage is increased. And as the voltage is ramped back down, the current retraces the steady-state curve. When the compartments are weakly coupled with the control value of the coupling conductance, however, the current does not strictly follow the steady-state curve. When the voltage passes the knee at I_{onset}, instead of sampling the distorted negative-slope region, the current shows a discontinuous drop to the depolarized or right-most branch of the steady-state curve. After the jump, the current tracks along the right-most branch as the voltage is increased further. When the voltage is ramped back down, the current remains on this branch, past the point where the current jumped down on the up ramp, until the knee at I_{offset} is reached. At this point, the current abruptly jumps up to the hyperpolarized or left-most branch, again repelled by the negative-slope region. As the voltage is ramped back down to rest, the current is the same as measured on the up ramp. In contrast to the theoretical steady-state *I-V* curve computed with the model, the *I-V* curve determined by voltage-clamp ramp does not show a negative-slope region but, instead, discontinuous jumps in current are observed at the voltage levels bounding this region.

The correspondence between the plateau thresholds and the steady-state *I-V* curve is further illustrated in Fig. 8, *C* and *D*, where the current at the soma is clamped rather than the voltage (control g_c value). In this simulation, the current is ramped up from zero, through I_{onset} and then ramped back down past I_{offset}. The time courses of the soma voltage and current are shown in Fig. 8*D* (*top* and *bottom trace*, respectively), whereas the same trajectory is displayed in Fig. 8*C* in the *I-V* plane (solid; arrows indicate direction of the current). As evident in Fig. 8*C*, the current is ramped sufficiently slowly so that the voltage trajectory essentially follows the theoretical steady-state *I-V* curve (dashed). The current ramp starts at zero current and resting voltage on the left-most branch of the theoretical *I-V* curve. As the current increases, the voltage increases along the branch until the current passes through I_{onset}. At this point, the plateau is activated (indicated by the arrow in Fig. 8*D*) by the voltage jumping from the left-most to the right-most branch of the theoretical *I-V* relation. As expected under current-clamp conditions, voltages on the distorted negative-slope region are not sampled. When the current is ramped back down, the voltage remains depolarized until the current passes through I_{offset} and the voltage jumps from the right-most to the left-most branch. From Fig. 8*C*, it is clear that the plateau thresholds are more precisely defined as the points where the slope of the steady-state *I-V* curve is zero. The curves in Fig. 7 showing the changes in plateau thresholds I_{onset} and I_{offset} were computed by tracking these points of zero slope, or saddle-node bifurcation points, as the maximum K(Ca) and L-like Ca^{2+} conductance values were varied (see APPENDIX).

Delays in plateau onset

In this section, we investigate several features of the activation time course of the plateau potential that have been

thought to reflect a slow activation time constant of the L-like Ca^{2+} conductance, perhaps on the order of 100 ms (Powers 1993; Schwindt and Crill 1984). In both experiments and the model, plateau potentials show significant delays in onset, in some cases lasting >1 s, in response to near-threshold current steps. For example, as seen in Fig. 6*A*, both the soma and dendritic voltages linger near subthreshold levels for hundreds of milliseconds before rising to the plateau state. Another feature observed both experimentally and in the model is that the length of the delay is sensitive to current step amplitude, with the delay decreasing substantially for small increases in current amplitude.

In the model, we obtained delays in plateau onset of appropriate durations for a relatively fast time constant (τ_{m_L} = 40 ms). Furthermore, analysis of the model and of our previous minimal model indicates that the delays in plateau onset may be observed when the inward current underlying the plateau activates rapidly, even instantaneously (Booth and Rinzel 1996). To understand the delays in plateau onset, we consider the soma voltage trajectory during plateau activation in the *I-V* plane, where current is measured in the soma compartment, as shown in Fig. 8*A*. In response to current steps of amplitude less than I_{onset}, the voltage approaches a stable, subthreshold level (cf. Fig. 6*A*) located on the left-most branch of the steady-state *I-V* curve. If, on the other hand, the current is stepped well above I_{onset}, the voltage quickly approaches the depolarized, plateau level defined on the right-most branch of the steady-state *I-V* curve for that current value. However, if the current is stepped to a value just above I_{onset}, the voltage moves toward the plateau state located on the right-most branch of the steady-state *I-V* curve, but passes very close to the knee at I_{onset}. At the knee, the slope conductance is zero; hence the voltage increases very slowly in its vicinity.

This slow passage near the knee at I_{onset} is shown in Fig. 9, which plots the model's response in the *I-V* plane to an applied current step just greater than I_{onset} (I_{app} = 15 $\mu A/cm^2$, compare with trajectory in Fig. 6*A*). Each dot in the figure corresponds to the voltage and current levels at 100-ms time intervals during the simulation. Initially, applied current is zero and the voltage is at its rest value located on the left-most branch of the steady-state *I-V* curve. In response to the current step, the voltage quickly moves to values near the knee at I_{onset}. The voltage slowly increases past the knee then rises more quickly to the depolarized plateau state on the right-most branch of the *I-V* curve.

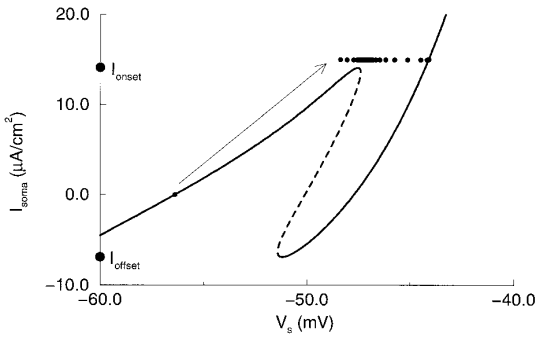

FIG. 9. Delayed plateau onset in simulated TTX and 5-HT caused by slow passage near knee of steady-state *I-V* curve at I_{onset}. Model response to applied current step of amplitude just above I_{onset} (I_{app} = 15 $\mu A/cm^2$; see Fig. 6*A*) plotted in somatic *I-V* plane under simulated TTX and 5-HT [g_{Na} = 0; soma $g_{K(Ca)}$ = 3.136; dendrite $g_{K(Ca)}$ = 0.69 mS/cm^2]. Theoretical steady-state *I-V* curve (solid/dashed) plotted for reference. Each dot denotes somatic voltage and membrane current at 100-ms time intervals during the simulation.

In dynamical systems theory, the knee in the steady-state *I-V* curve is called a saddle-node bifurcation point of the model's steady-state solution set. The deceleration of trajectories as they pass near a saddle-node point is a well-known phenomenon, and classical bifurcation analysis has determined that the delay in plateau onset caused by the slow passage near a saddle-node depends on current step amplitude in the following manner

$$\text{Delay in Plateau Onset} \propto \frac{1}{\sqrt{I_{app} - I_{onset}}}$$

where I_{app} is the current step amplitude (see Booth and Rinzel 1996; Strogatz 1994). From this relation, the sensitivity of the delay to current step amplitude is clear. For current steps very close to I_{onset}, the delay can be significant, but it falls off quickly as the amplitude increases above threshold. This relation was determined for an instantaneously activating inward current underlying the plateau. Simulations with our model have indicated that the finite activation time of the L-like Ca^{2+} conductance exaggerates the delay in plateau onset so that it is even greater than predicted by the above formula. Furthermore, the finite activation time makes long delays more robust to current step amplitude, so that a substantial delay, on the order of several hundred milliseconds, may still be observed in response to current steps much larger than I_{onset}.

A final feature of plateau activation that is observed experimentally and that is obtained in the model with a relatively fast activation time constant for I_{Ca-L} is the slow rise of the voltage to the plateau state once plateau activation has been initiated. Simulations investigating the effects of longer activation time constants revealed that the slope of the voltage transition to the plateau depends nonlinearly on the activation time constant, so that it is much shallower than a linear dependence would predict. Accordingly, the transition slopes were surprisingly shallow with activation time constants on the order of 100 ms. One aspect of this voltage transition to the plateau that our model does not account for, however, is the subtle decrease in the slope of the transition that is experimentally observed as current step amplitude is decreased toward threshold (compare Fig. 6*A* with Fig. 3*A* in Hounsgaard and Kiehn 1989) (see DISCUSSION).

DISCUSSION

Comparison with previous motoneuron models

Previous motoneuron models have concentrated on understanding normal firing behavior (see Binder et al. 1996 for a review) and 5-HT–induced bistable firing patterns (Booth and Rinzel 1995; Gutman 1991; Lee and Heckman 1996a; Powers 1993), but the present model is the first to address the systematic development of complex and bistable firing patterns by appropriate simulation of multiple ion channel blockers and neurotransmitters. As part of a larger study of motoneuron firing behavior with a threshold-crossing model, Powers (1993) obtained maintained firing following a short-lasting current pulse but never true bistable firing patterns

when parameters were varied from their control values. Interestingly, in contrast to our findings, it was not possible in Powers' (1993) model to induce plateau potentials by reducing potassium currents alone. The necessary changes were a simultaneous reduction of outward currents and increases in the time constants for activation of a persistent, low-threshold calcium conductance and a slow, potassium conductance. These differences to our model might be explained by the single compartment structure of Powers' model, since in our model the spatial segregation of the soma and dendrites was an essential parameter determining plateau development (see *How realistic is the model?*) (Booth and Rinzel 1995).

The contribution of dendritic conductances to plateau generation and the ensuing bistable firing patterns has also been previously investigated in an equivalent cylinder, cable model (Gutman 1991) and in two-compartment models (Booth and Rinzel 1995; Lee and Heckman 1996a). In these models, plateau-generating currents were not slow and were localized in the dendrites (cable or compartment, respectively), and the pharmacologically mediated state change from the normal situation when the plateau is masked to the plateau-generating state was not addressed. In addition, the ionic conductances responsible for spike and plateau generation in some of these models were idealized and not biophysically grounded (Booth and Rinzel 1995; Gutman 1991). We therefore believe that the present model represents a valuable addition to previously published models of vertebrate motoneurons by combining a compartmental structure with nonuniform spatial distribution of biophysically plausible active conductances.

How realistic is the model?

Although the model displays a variety of behaviors resembling experimental results during simulations of different pharmacological conditions, it does not constitute a physiologically complete description of a vertebrate motoneuron. The types of ionic conductances included in the model are biophysically plausible, but, with only limited quantitative data available from turtle motoneurons, their distribution between the soma and dendrite compartments and their kinetic parameters have been qualitatively determined. However, the kinetic parameters do not significantly differ from those quantitatively identified in cat motoneurons (Binder et al. 1996; Schwindt and Crill 1984). Our model also does not include several conductances that have been identified in vertebrate motoneurons, such as a hyperpolarization-activated inward, or ''sag,'' current (I_h) (Bayliss et al. 1994; Schwindt and Crill 1984; Takahashi 1990a,b) and an A-type potassium current (I_A) (Takahashi 1990b; Viana et al. 1993b). In crustacean and neonatal rat spinal motoneurons, I_h is active at resting membrane potentials and is enhanced by 5-HT (Kiehn and Harris-Warrick 1992a; Takahashi and Berger 1990). Given its important role in plateau generation in crustacean motoneurons (Kiehn and Harris-Warrick 1992a,b), I_h is a natural candidate for inclusion in future models as is a low-threshold, transient calcium current that is found in neonatal rat motoneurons and that plays a role in rebound excitation (Berger and Takahashi 1990). Currently, very little is known about I_A in vertebrate motoneurons (see Binder et al. 1996; McLarnon 1995), hence it was omitted from the model.

Our model, in addition, only qualitatively represents the nonuniform distribution of ionic conductances over soma and dendrites by lumping currents into two, not strongly coupled compartments. Studies with this model and our previous, more simplified model (Booth and Rinzel 1995) have supported the hypothesis that the bistable firing patterns invoked by 5-HT require a nonuniform distribution of ionic conductances and, specifically, a segregation of plateau-generating currents from spike-generating currents. As indicated by Gutman's (1991) results with an idealized cable model, preliminary simulations with multicompartmental representations of the dendrites have shown that bistable firing patterns can be obtained when plateau-generating currents are more widely distributed over several compartments rather than lumped into a single compartment. Furthermore, other simulations confirm that the spike- and plateau-generating currents need not be entirely segregated to obtain the bistable behaviors. In particular, in the present model, when I_{Ca-L} is included in the soma compartment, in similar densities as it appears in the dendrite compartment, results identical to those presented here are obtained.

Mechanism for plateau generation

Although our model might not provide a complete description of vertebrate motoneuron membrane properties, it allowed us to test specific hypotheses on the effects of pharmacological perturbations. For example, experimental results have suggested that plateau potential behavior may be evoked by sufficient reduction of various combinations of outward, potassium currents. Our model simulations of high-concentration TEA and apamin experiments, however, have challenged this assumption and, as we will argue, suggest that the primary currents balancing the plateau-generating calcium conductance are calcium-dependent potassium conductances. The experimental results in apamin determine that a K(Ca) conductance contributes to plateau masking (Hounsgaard and Mintz 1988). The model results in simulated apamin confirm that $I_{K(Ca)}$ participates in plateau masking. Furthermore, in the model, the influence of the K(Ca) conductance on the plateau is very robust: increasing dendritic $I_{K(Ca)}$ will always mask the plateau, whereas decreasing it easily unmasks the plateau. In the high TEA experiments, it was suggested that blocking I_{K-dr} alone may also release the plateau (Hounsgaard and Mintz 1988). We have used the model to investigate this possible action of TEA. Our simulations have shown that a large level of dendritic I_{K-dr} is needed to mask the plateau. Moreover, this necessary conductance level is sufficiently large as to maintain plateau block even under simulated apamin, when K(Ca) conductances are completely removed. Hence, to obtain all pharmacological behaviors, the high-concentration TEA experiments cannot be simulated by only decreasing the delayed potassium rectifier. So, in contrast to the real experiments, we find that both K^+ delayed rectifier and K(Ca) conductances must be decreased. These results also suggest that the delayed rectifier conductance in the dendrite cannot be large, because it would impede the plateau in the apamin simulations (we have elected to eliminate it entirely). We thus conclude that in turtle motoneurons the primary outward currents balancing the plateau-generating calcium conductance are calcium-dependent potassium conductances.

Furthermore, proceeding from this conclusion, the pharmacological evidence implies that the K(Ca) currents are mediated by ion channels that are sensitive to either TEA in high concentrations or apamin and 5-HT. An apamin-sensitive K(Ca) conductance has been identified in turtle motoneurons (Hounsgaard et al. 1988b), which corresponds to the low-conductance SK channel described in other neurons, where it also generates a medium to slow duration AHP, as in the turtle neuron (see McLarnon 1995). The model results, then, suggest that turtle motoneurons may contain two Ca^{2+}-dependent K^+ conductances, one of which is TEA sensitive. (Note that in the model they are represented by 1 conductance.) Such a TEA-sensitive K(Ca) conductance has indeed been described in hypoglossal motoneurons where it may contribute to spike repolarization (Viana et al. 1993b).

Investigation of 5-HT modulation

An advantage offered by the simulation of pharmacological agents is that the effects on firing patterns of different concentrations of the agent can be investigated. In the experimental preparation, the time necessary for the effects of an agent to reach steady state and the difficulty in obtaining precise quantitative measurements of plateau-generating ability over time prohibit this type of systematic measurement. With the model, however, we are able to monitor the development of complex behaviors as not only different concentrations of a pharmacological agent are simulated but also as different effects of the agent on ionic conductances are simulated. We particularly examined the development of plateau properties obtained in TTX as application of 5-HT is simulated. Our comparison of plateau onset thresholds under 5-HT enhancement of the plateau-generating, L-like calcium conductance and reduction of $I_{K(Ca)}$ (Fig. 7*B*) illustrate that 5-HT may invoke plateau behavior through a combination of actions on more than one conductance. Although the effect on $I_{K(Ca)}$ has been demonstrated experimentally (Hounsgaard and Kiehn 1989), there is as yet no experimental evidence for a 5-HT modulation of I_{Ca-L} in turtle motoneurons.

In our model, we have simulated the effect of 5-HT as a direct inhibition of the K(Ca) conductance. It remains a possibility, as has been demonstrated in hypoglossal motoneurons (Bayliss et al. 1995), that 5-HT indirectly reduces $I_{K(Ca)}$ by blocking N-like calcium channels. Although a thorough study of this effect of 5-HT has not been performed, preliminary simulations with the present ''control case'' parameters indicate that this indirect reduction of $I_{K(Ca)}$ is not sufficient to unmask plateau properties. Also, in this study, we have simulated the 5-HT enhancement of the L-like Ca^{2+} current as an increase in its maximum conductance, thereby implying that 5-HT recruits L-like Ca^{2+} channels. Another possible action of 5-HT that results in enhancement of I_{Ca-L} is a hyperpolarizing or left shift of the steady-state half-activation voltage for the activation gate. Model results similar to those in Fig. 7 but with 5-HT simulated by a left shift of the half-activation of I_{Ca-L} by 1 or 2 mV show that plateau potentials can be obtained with less reduction of $I_{K(Ca)}$ than for the control parameters of I_{Ca-L}. Furthermore, the results indicate that I_{onset} is fairly sensitive to the half-activation voltage, specifically, I_{onset} is much smaller when the half-activation is left-shifted by a few millivolts. These types of analyses clearly demonstrate that the model can be used as a predictive tool to investigate modulatory effects of pharmacological agents and to formulate future experiments.

Delay and slope of plateau activation

The model allowed a thorough investigation of the time course of plateau activation. The results indicated that although delays in plateau onset are a general feature of plateau potentials irregardless of the activation gating rate of the plateau-generating currents, the steepness of the time course of the voltage transition from subthreshold to plateau states does depend on the underlying current's activation rate. This model result does not, however, completely account for the experimental behavior of the voltage transition to the plateau. Plateaus in turtle motoneurons show an additional subtle increase in the steepness of the voltage transition as the current is stepped away from onset threshold, a behavior that is not observed in the model (compare Fig. 6 with Hounsgaard and Kiehn 1989, Fig. 3). In turtle dorsal horn neurons, plateau potentials, mediated by an L-type Ca^{2+} conductance, show, in addition to delays in onset and slow transitions to the plateau state, wind-up in response to preceding depolarization, suggesting a depolarization-induced warm-up of the L-type conductance (Russo and Hounsgaard 1996). Warm-up is present in motoneurons as well (Svirskis and Hounsgaard 1995), and it is likely that the subtle increase in the voltage transition slope observed when the step amplitude is increased is due to a depolarizing induced warm-up of the L-like calcium channels, implying that there are at least two mechanisms contributing to the slope of the voltage transition.

APPENDIX

The current balance equations for the two compartments are

$$C_m \frac{dV_S}{dt} = -g_{Na} m_\infty^3(V_S) h (V_s - V_{Na}) - g_{K-dr} n^4 (V_S - V_K) - g_{Ca-N} m_N^2 h_N (V_S - V_{Ca}) - g_{K(Ca)} \frac{Ca_S}{(Ca_S + K_d)} (V_S - V_k) - g_L (V_S - V_L) + \frac{g_c}{p} (V_D - V_S) + I_{app}$$

$$C_m \frac{dV_D}{dt} = -g_{Ca-N} m_N^2 h_N (V_D - V_{Ca}) - g_{Ca-L} m_L (V_D - V_{Ca}) - g_{K(Ca)} \frac{Ca_D}{(Ca_D + K_d)} (V_D - V_K) - g_L (V_D - V_L) + \frac{g_c}{1 - p} (V_S - V_D)$$

where V_x (in mV) is the voltage and Ca_x (in μM) is the intracellular Ca^{2+} concentration in the soma ($x = S$) and dendrite ($x = D$) compartments. The electronic-like properties between the two compartments are determined by the coupling conductance, g_c, which regulates current flow between the compartments and the parameter p, which is the ratio of somatic surface area to total cell surface area; in this study, $g_c = 0.1$ mS/cm^2 and $p = 0.1$. An applied current, I_{app} (in μA/cm^2), may be injected into the soma compartment. The Ca^{2+}-dependent K^+ conductance is an instantaneous function of intracellular Ca^{2+} concentration, which is half-saturated at concentration levels of $K_d = 0.2$ μM. To ease the notational

burden, we have not distinguished with symbols the maximal ionic conductances, although their values differ, in the soma and dendrite compartments.

The gating kinetics of the ionic conductances are governed by equations of the following form

$$\frac{dw}{dt} = \frac{w_\infty(V) - w}{\tau_w}$$

where the steady-state activation and inactivation functions are given by

$$w_\infty(V) = \frac{1}{1 + \exp[(V - \theta_w)/k_w]}$$

where w is h for sodium inactivation, n for K^+ delayed rectifier activation, m_N and h_N for N-like Ca^{2+} activation and inactivation, respectively, and m_L for L-like Ca^{2+} activation.

The half-activation and half-inactivation voltages for the gating functions are (in mV) $\theta_m = -35$, $\theta_h = -55$, $\theta_n = -28$, $\theta_{mN} = -30$, $\theta_{hN} = -45$, and $\theta_{mL} = -40$. The activation and inactivation sensitivities for the gating functions are (in mV) $k_m = -7.8$, $k_h = 7$, $k_n = -15$, $k_{mN} = -5$, $k_{hN} = 5$, and $k_{mL} = -7$. The activation and inactivation time constants for the Ca^{2+} conductances are given by the following constants (in ms): $\tau_{mN} = 4$, $\tau_{hN} = 40$, and $\tau_{mL} = 40$. The time constants for sodium inactivation and K^+ delayed rectifier activation are voltage-dependent functions defined as follows (in ms): $\tau_h(V) = 30/\{\exp[(V + 50)/15] + \exp[-(V + 50)/16]\}$ and $\tau_n(V) = 7/\{\exp[(V + 40)/40] + \exp[-(V + 40)/50]\}$.

Intracellular calcium concentration in the either compartment (Ca_x, for $x = S$ or D, in μM) depends on the total compartment Ca^{2+} current, I_{Ca}, in the following manner

$$\frac{dCa_x}{dt} = f[-\alpha I_{Ca} - k_{Ca}Ca_x]$$

In the soma compartment, the total Ca^{2+} current is mediated by the N-like Ca^{2+} conductance, whereas in the dendrite compartment both the N-like and L-like Ca^{2+} conductances contribute to the total Ca^{2+} current. The constant $f = 0.01$ is the percent of free to bound Ca^{2+} (Helmchen et al. 1996), $\alpha = 0.009$ mol/C/μm converts the total Ca^{2+} current, I_{Ca}, to Ca^{2+} concentration and $k_{Ca} = 2$ ms^{-1} is the Ca^{2+} removal rate.

The reversal potentials for the ionic currents are $V_{Na} = 55$ mV, $V_K = -80$ mV, and $V_{Ca} = 80$ mV. The leak conductance density in each compartment is $g_L = 0.51$ mS/cm^2, and the leak reversal potential is $V_L = -60$ mV. The membrane capacitance is $C_m = 1$ μF/cm^2. Control values of the maximum ionic conductance densities are given in Table 1, and their modulated values corresponding to the pharmacological simulations displayed in Figs. 2–9 are given in the corresponding figure captions.

To better understand the contribution of the different ionic conductances in the generation of an AP, Fig. A1 displays the individual ionic currents (*bottom panel*) measured during one of the control case APs displayed in Fig. 2*A* (soma voltage shown in *top panel*). The fast upstroke of the AP is driven by the sodium current, I_{Na} (solid), whose peak is truncated in the figure. The spike is repolarized by inactivation of the Na^+ conductance and activation of the K^+ delayed rectifier current, I_{K-dr} (dashed). I_{K-dr} is also responsible for the fast AHP following the spike, indicated by the dip in voltage below the resting potential (*top panel*, dashed line). The dip in I_{Na} after its peak is caused by a decrease in driving force near the peak of the voltage spike. The slower activating N-like Ca^{2+} current, I_{Ca-N} (dotted-dashed), peaks as I_{Na} returns to zero, increasing the width of the AP and activating the Ca^{2+}-dependent K^+ current, $I_{K(Ca)}$ (dotted). Activation of $I_{K(Ca)}$ occurs as I_{K-dr} decays, initiating the slow AHP and governing the return to spike threshold. Note, the brief peak of $I_{K(Ca)}$ (coincident with the AP peak) is due to the large driving potential and not to a rise in Ca^{2+} concentration, which occurs later, driven by I_{Ca-N}.

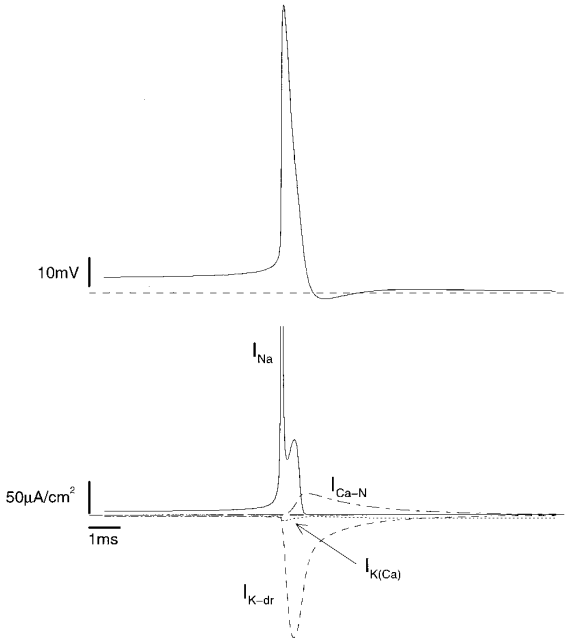

FIG. A1. Dissection of individual ionic currents contributing to generation of an action potential. *Top panel*: soma voltage measured during action potential generated in response to current step $I_{app} = 6$ μA/cm^2, as in Fig. 2*A*. Dashed line indicates resting potential. *Bottom panel*: ionic currents in soma compartment during action potential [solid, I_{Na}; dashed, I_{K-dr}; dot-dashed, I_{Ca-N}; dotted, $I_{K(Ca)}$], measured as deviations from 0 μA/cm^2 (long dashed).

The model equations were numerically integrated using a program XPP, written by G. B. Ermentrout, which offers a variety of integration methods and can be run on any UNIX workstation. The model results in Figs. 2–6 and Fig. A1 were obtained by integrating the equations with a variable time step Gear method (tolerance = 0.004, maximum time step = 0.05 ms). The theoretical steady-state *I-V* curves shown in Figs. 8 and 9, and the continuous tracking of the plateau thresholds shown in Fig. 7 were computed with the bifurcation analysis program AUTO (Doedel 1981) through its interface with XPP.

O. Kiehn acknowledges the support of the Novo Nordic Foundation and the Danish Medical Research Council.

Present address of J. Rinzel: Center for Neural Science and Courant Institute of Mathematical Sciences, New York University, 4 Washington Place, Room 809, New York, NY 10003. Information on the XPP program written by G. B. Ermentrout may be obtained at the World Wide Web site http://www.pitt.edu/~phase, and the program itself is available via anonymous ftp from ftp.math.pitt.edu/pub/bardware.

Present address and address for reprint requests: V. Booth, Dept. of Mathematics, New Jersey Institute of Technology, University Heights, Newark, NJ 07102-1982.

Received 30 August 1996; accepted in final form 2 September 1997.

REFERENCES

BALDISSERA, F. AND GUSTAFSSON, B. Regulation of repetitive firing in motoneurons by the afterhyperpolarization conductance. *Brain Res.* 30: 431–434, 1974.

BAYLISS, D. A., UMEMIYA, M., AND BERGER, A. J. Inhibition of N- and P-type calcium currents and the after-hyperpolarization in rat motoneurons by serotonin. *J. Physiol. (Lond.)* 485: 635–647, 1995.

BAYLISS, D. A., VIANA, F., BELLINGHAM, M. C., AND BERGER, A. J. Characteristics and post-natal development of a hyperpolarization-activated in-

ward current in rat hypoglossal motoneurons in vitro. *J. Neurophysiol.* 71: 119–128, 1994.

BERGER, A. J. AND TAKAHASHI, T. Serotonin enhances a low-voltage–activated calcium current in rat spinal motoneurons. *J. Neurosci.* 10: 1922–1928, 1990.

BINDER, M. D., HECKMAN, C. J., AND POWERS, R. K. The physiological control of motoneuron activity. In: *Handbook of Physiology. Exercise: Regulation and Integration of Multiple Systems.* Bethesda, MD: Am. Physiol. Soc., 1996, sect. 12, p. 3–53.

BOOTH, V. AND RINZEL, J. A minimal, compartmental model for a dendritic origin of bistability of motoneuron firing patterns. *J. Comput. Neurosci.* 2: 299–312, 1995.

BOOTH, V. AND RINZEL, J. Plateau potentials in bistable motoneurons. In: *Computational Neuroscience: Trends in Research 1995*, edited by J. M. Bower. New York: Academic, 1996, p. 47–52.

BOOTH, V., RINZEL, J., AND KIEHN, O. A compartmental model of bistable and complex firing patterns of vertebrate motoneurons. *Soc. Neurosci. Abstr.* 22: 725.4, 1996.

BURKE, R. E., FYFFE, R.E.W., AND MOSCHOVAKIS, A. K. Electrotonic architecture of cat gamma motoneurons. *J. Neurophysiol.* 72: 2302–2316, 1994.

CONWAY, B. A., HULTBORN, H., KIEHN, O., AND MINTZ, I. Plateau potentials in α-motoneurones induced by intravenous injection of L-DOPA and clonidine in the spinal cat. *J. Physiol. (Lond.)* 405: 369–384, 1988.

DOEDEL, E. J. AUTO: a program for the automatic bifurcation analysis of autonomous systems. *Congressus Numerantium* 30: 265–284, 1981.

EKEN, T. AND KIEHN, O. Bistable firing properties of soleus motor units in unrestrained rats. *Acta Physiol. Scand.* 136: 383–394, 1989.

GUTMAN, A. M. Bistability of dendrites. *Int. J. Neural Syst.* 1: 291–304, 1991.

HELMCHEN, F., IMOTO, K., AND SAKMANN, B. Ca^{2+} buffering and action potential–evoked Ca^{2+} signaling in dendrites of pyramidal neurons. *Biophys. J.* 70: 1069–1081, 1996.

HOUNSGAARD, J., HULTBORN, H., JESPERSON, B., AND KIEHN, O. Bistability of α-motoneurones in the decerebrate cat and in the acute spinal cat after intravenous 5-hydroxytryptophan. *J. Physiol. (Lond.)* 405: 345–367, 1988a.

HOUNSGAARD, J. AND KIEHN, O. Ca^{++} dependent bistability induced by serotonin in spinal motoneurons. *Exp. Brain Res.* 57: 422–425, 1985.

HOUNSGAARD, J. AND KIEHN, O. Serotonin-induced bistability of turtle motoneurones caused by a nifedipine-sensitive calcium plateau potential. *J. Physiol. (Lond.)* 414: 265–282, 1989.

HOUNSGAARD, J. AND KIEHN, O. Calcium spikes and calcium plateaux evoked by differential polarization in dendrites of turtle motoneurones in vitro. *J. Physiol. (Lond.)* 468: 245–259, 1993.

HOUNSGAARD, J., KIEHN, O., AND MINTZ, I. Response properties of motoneurons in a slice preparation of the turtle spinal cord. *J. Physiol. (Lond.)* 398: 575–589, 1988b.

HOUNSGAARD, J. AND MINTZ, I. Calcium conductance and firing properties of spinal motoneurones in the turtle. *J. Physiol. (Lond.)* 398: 591–603, 1988.

JACK, J.J.B., NOBLE, D., AND TSIEN, R. W. *Electric Current Flow in Excitable Cells.* New York: Oxford Univ. Press, 1983.

KERNELL, D. The adaptation and the relation between discharge frequency and current strength of cat lumbosacral motoneurones stimulated by long-lasting injected currents. *Acta Physiol. Scand.* 65: 65–73, 1965.

KERNELL, D. AND MONSTER, A. W. Timecourse and properties of late adaptation in spinal motoneurones of the cat. *Exp. Brain Res.* 46: 191–196, 1982.

KIEHN, O. Electrophysiological effects of 5-HT on vertebrate motoneurones. In: *Aspects of Synaptic Transmission: LTP, Galanin, Opioids, Autonomic and 5-HT*, edited by T. W. Stone. London: Taylor & Francis, 1991a, p. 330–357.

KIEHN, O. Plateau potentials and active integration in the ''final common pathway'' for motor behavior. *Trends Neurosci.* 14: 68–73, 1991b.

KIEHN, O., ERDAL, J., EKEN, T., AND BRUHN, T. Selective depletion of spinal monoamines changes the rat soleus EMG from a tonic to a more phasic pattern. *J. Physiol. (Lond.)* 492: 173–184, 1996.

KIEHN, O. AND HARRIS-WARRICK, R. M. Serotonergic stretch receptors induce plateau properties in a crustacean motor neuron by a dual-conductance mechanism. *J. Neurophysiol.* 68: 485–495, 1992a.

KIEHN, O. AND HARRIS-WARRICK, R. M. 5-HT modulation of hyperpolarization-activated inward current and calcium-dependent outward current in a crustacean motor neuron. *J. Neurophysiol.* 68: 496–508, 1992b.

LEE, R. H. AND HECKMAN, C. J. Dendritic plateau potentials and bistable firing in spinal motoneurons: computer simulation studies. *Soc. Neurosci. Abstr.* 22: 725.5, 1996a.

LEE, R. H. AND HECKMAN, C. J. Influence of voltage-sensitive dendritic conductances on bistable firing and effective synaptic current in cat spinal motoneurons in vivo. *J. Neurophysiol.* 76: 2107–2110, 1996b.

LÜSCHER, H. R. AND CLAMANN, H. P. Relation between structure and function in information transfer in spinal monosynaptic reflex. *Physiol. Rev.* 72: 71–99, 1992.

MCLARNON, J. G. Potassium currents in motoneurones. *Prog. Neurobiol.* 47: 513–531, 1995.

NITZAN, R., SEGEV, I., AND YAROM, Y. Voltage behavior along the irregular dendritic structure of morphologically and physiologically characterized vagal motoneurons in guinea pig. *J. Neurophysiol.* 63: 333–346, 1990.

PINSKY, P. F. AND RINZEL, J. Intrinsic and network rhythmogenesis in a reduced Traub model for CA3 neurons. *J. Comput. Neurosci.* 1: 39–60, 1994.

POWERS, R. K. A variable-threshold motoneuron model that incorporates time- and voltage-dependent potassium and calcium conductances. *J. Neurophysiol.* 70: 246–262, 1993.

RUSSO, R. E. AND HOUNSGAARD, J. Plateau-generating neurones in the dorsal horn in an in vitro preparation of the turtle spinal cord. *J. Physiol. (Lond.)* 493: 39–54, 1996.

SCHWINDT, P. C. AND CALVIN, W. H. Membrane-potential trajectories between spikes underlying motoneuron firing rates. *J. Neurophysiol.* 35: 311–325, 1972.

SCHWINDT, P. C. AND CRILL, W. E. Role of a persistent inward current in motoneuron bursting during spinal seizures. *J. Neurophysiol.* 43: 1296–1318, 1980a.

SCHWINDT, P. C. AND CRILL, W. E. Properties of a persistent inward current in normal and TEA-injected motoneurons. *J. Neurophysiol.* 43: 1700–1724, 1980b.

SCHWINDT, P. C. AND CRILL, W. E. Effects of barium on cat spinal motoneurons studied by voltage clamp. *J. Neurophysiol.* 44: 827–846, 1980c.

SCHWINDT, P. C. AND CRILL, W. E. Membrane properties of cat spinal motoneurons. In: *Handbook of the Spinal Cord*, edited by R. Davidoff, R. New York: Dekker, 1984, p. 199–242.

STROGATZ, S. H. *Nonlinear Dynamics and Chaos.* New York: Addison-Wesley, 1994.

SVIRSKIS, G. AND HOUNSGAARD, J. Depolarization-induced facilitation on 1-type Ca^{2+} channels underlies slow kinetics of plateau potentials in turtle motoneurons. *Soc. Neurosci. Abstr.* 21: 65, 1995.

TAKAHASHI, T. Membrane currents in visually identified motoneurones of neonatal rat spinal cord. *J. Physiol. (Lond.)* 423: 27–46, 1990a.

TAKAHASHI, T. Inward rectification in neonatal rat spinal motoneurones. *J. Physiol. (Lond.)* 423: 47–62, 1990b.

TAKAHASHI, T. AND BERGER, A. J. Direct excitation of rat spinal motoneurones by serotonin. *J. Physiol. (Lond.)* 423: 63–76, 1990.

TRAUB, R. D. Motorneurons of different geometry and the size principle. *Biol. Cybern.* 25: 163–176, 1977.

TRAUB, R. D. AND LLINAS, F. The spatial distribution of ionic conductances in normal and axotomized motorneurons. *Neuroscience* 2: 829–849, 1977.

UMEMIYA, M. AND BERGER, A. J. Properties and function of low- and high-voltage-activated Ca^{2+} channels in hypoglossal motoneurons. *J. Neurosci.* 14: 5652–5660, 1994.

VIANA, F., BAYLISS, D. A., AND BERGER, A. J. Calcium conductances and their role in the firing behavior of neonatal rat hypoglossal motoneurons. *J. Neurophysiol.* 69: 2137–2149, 1993a.

VIANA, F., BAYLISS, D. A., AND BERGER, A. J. Multiple potassium conductances and their role in action potential repolarization and repetitive firing behavior of neonatal rat hypoglossal motoneurons. *J. Neurophysiol.* 69: 2150–2163, 1993b.

ZHANG, L. AND KRNJEVIC, K. Apamin depresses selectively the after-hyperpolarization of cat spinal motoneurones. *Neurosci. Lett.* 74: 58–62, 1987.